MICHIGAN STATE UNIVERSITY

CYCLOTRON LABORATORY

EXTENDED PWBA TREATMENT OF THE $^{6}Li + {}^{6}Li \rightarrow 2\alpha + 2d$ REACTION

ROBERT E. WARNER

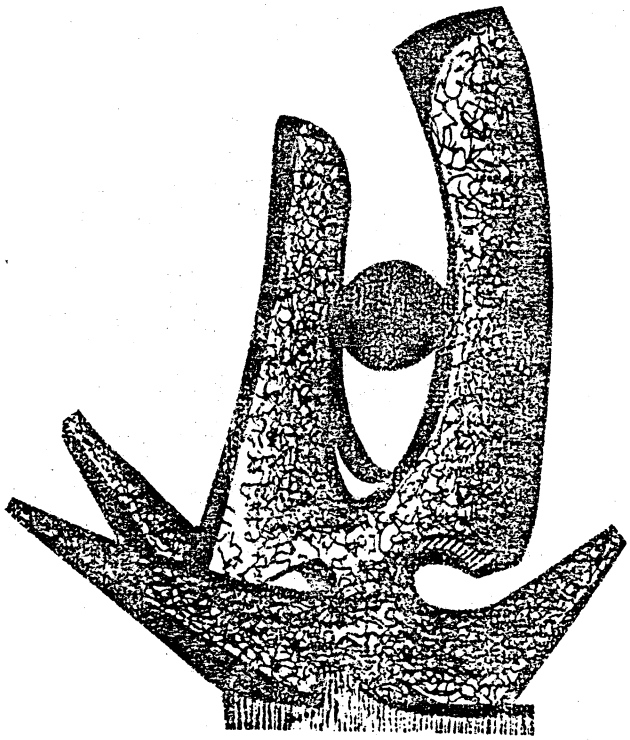

JULY 1981

MSUCL-354

MSUCL-354
July 1981

Extended PWBA Treatment of the $^6Li + {}^6Li \to 2\alpha + 2d$ Reaction

Robert E. Warner[+]

Cyclotron Laboratory
Michigan State University,[++]
East Lansing, MI 48824 USA

ABSTRACT

Recent double coincidence data for the $^6Li + {}^6Li \to 2\alpha + 2d$ reaction show double spectator pole (DSP) peaks much sharper than those predicted from realistic ^6Li cluster wave functions. The PWBA correctly predicts the centers and approximate amplitudes of these peaks. However their widths remain much too large even when all obvious straightforward improvements -- symmetry under boson exchange, Coulomb cluster wave functions, a finite-range participant interaction potential, and deuteron structure -- are added to the model.

[+] Visiting Professor, 1980-81. Permanent address: Oberlin College, Oberlin, OH 44074, USA.

[++] Research supported by the National Science Foundation under Grant No. Phy 78-22696.

1. Introduction

Nuclear spectator phenomena are studied from two complementary viewpoints. Deuteron breakup by fast protons was observed by Kuckes et al.[1] two decades ago. Quasi-free p-p scattering (QFS) was found to be an important reaction mechanism, and the lab momentum spectrum of the (spectator) neutron was the same in the final state as in the initial deuteron. Their interpretive PWBA impulse approximation model and its subsequent extensions have been used to analyze QFS-type breakup and charge-exchange reactions among other light nuclei.[2-4] More recently, projectile fragments with velocities near the beam velocity have been observed[5-6] after collisions between heavy-ion pairs such as $^{16}O + {}^{208}Pb$ and $^{20}Ne + {}^{197}Au$. These results are interpreted by the participant-spectator model;[7] in particular, the momentum distribution of the spectator fragments is found from the Fermi gas model.[8]

^6Li projectiles are of particular interest since they have intermediate mass and a well-defined cluster structure.[2,9] Neumann et al.[10] detected p,d,t,^3He, and α-particles from 156 MeV ^6Li fragmentation on targets from ^{12}C to ^{208}Pb. Momentum widths consistent with the ^6Li ground-state wave function were obtained for the deuteron and α-particle groups. However, when 36 to 47 MeV $^6Li + {}^6Li$ double breakup was studied at Chalk River,[11] the d+d and $\alpha+\alpha$ coincidence spectra contained peaks whose momentum widths were 3 to 5 times smaller than expected. This suggested a highly peripheral reaction selecting clusters of atypically low momenta.

In the Chalk River experiment[11] hereafter referred to as I, the peaks occurred near double spectator pole (DSP) conditions: their locations were consistent with one fragment travelling with the beam velocity and the other remaining at rest in the laboratory. It was shown that these enhancements did not result from phase space, a ^{6}Li final-state interaction, or sequential decay of levels in ^{4}He, ^{6}Li, or ^{8}Be.

This paper seeks to determine whether any extension of the PWBA theory can explain the abnormally small momentum widths observed in I. We find that symmetrizing the matrix elements for exchange of identical bosons, including Coulomb effects in the ^{6}Li cluster wave functions, and including deuteron structure by treating the deuteron as two nucleons rather than a point cluster, all have negligible effect on the peak widths. The predicted widths depend only upon the rms cluster separation, not upon the specific form of the wave function (e.g., a gaussian wave function rather than that of a Woods-Saxon well). Similarly, in I, four different cluster wave functions were shown to overpredict the widths by equal amounts. Finally, in the PWBA theory, we show that predicted widths are nearly independent of the range of the participant interaction potential, but the peak centers shift appreciably from their observed locations if this range exceeds about 1 fm.

Even though the extended PWBA treatment fails dramatically to predict the peak widths observed in I, it gives a good account of the magnitude of the cross section. This suggests

that the reaction proceeds basically as described by the model, though possibly with some novel feature previously unobserved in light nuclear breakup. The DSP peaks (observed at 6 to 8 MeV/nucleon) could also represent an extreme case of the considerably broader spectator peaks seen in heavy ion collisions. McVoy and Nemes[12] interpret the increase of momentum peak widths through changes in the reaction mechanism: from transfer to fragmentation, or from prompt to delayed fragmentation as the energy rises. Since these momentum widths depend so strongly on both energy and the number of nucleons removed from the projectile, it would be worthwhile investigating whether the ^{6}Li double breakup and heavy ion observations are connected. This would require measurements for ^{6}Li + ^{6}Li collisions at higher energies, where we expect the peak widths to increase, and of collisions of ^{6}Li with other light nuclei. We note that fragmentation seems the only likely mechanism for ^{6}Li double breakup.

2. PWBA Theory, and Relationship of Four-Body and Elastic Cross Sections

In the experiments[11] which we seek to interpret, two identical bosons (i.e., two deuterons or two α-particles) of mass m_1 are detected at equal laboratory angles following $^6Li + {}^6Li$ double breakup. The other two bosons, of mass m_3, are not detected. We designate the detected particles ("participants") as 1 and 2 and the undetected ones ("spectators") as 3 and 4. Figure 1 shows the laboratory momenta ($\vec{P}_1$ through $\vec{P}_4$) of all four final nuclei and the velocity v_c of the undetected particles' center of mass. We let RCM be the frame of reference in which this center of mass is at rest. Thus, in Fig. 1 one undetected particle is emitted with polar angle γ, azimuthal angle ϕ, and momentum $\vec{P}_3$ in the RCM, and the other has $\vec{P}_4 = -\vec{P}_3$ in this frame. Measurements determine $\vec{P}_1$ and $\vec{P}_2$, and the magnitude of P_3 and P_4; however, γ and ϕ are completely undetermined. The PWBA theory for $^6Li + {}^6Li$ double breakup has been given elsewhere[11,13,14] but must be summarized here to place later developments in perspecitive. We initially consider ^6Li to consist of two structureless particles (α and deuteron) whose cluster wavefunction is ψ_L; in Sect. 6 we relax this assumption to take account of deuteron structure. All particles not bound to each other are considered not to interact and therefore are described by plane waves. Thus the initial and final wavefunctions for the system are:

$$|i\rangle = \psi_L(\vec{r}_1-\vec{r}_3)\psi_L(\vec{r}_2-\vec{r}_4)\exp\left(i(\vec{P}_0\cdot\vec{R}_{13})/\hbar\right) \quad (1)$$

and

$$\langle f| = \exp\left(i(\vec{P}_1\cdot\vec{r}_1 + \vec{P}_2\cdot\vec{r}_2 + \vec{P}_3\cdot\vec{r}_3 + \vec{P}_4\cdot\vec{r}_4)/\hbar\right) \quad (2)$$

where $\vec{P}_0$ is the projectile momentum and $\vec{R}_{13}$ is the displacement of its center of mass. The two participants are assumed to undergo quasi-free scattering (QFS) in a potential

$$V_{12} = V_G\exp\left(-(\vec{r}_1-\vec{r}_2)^2/r_o^2\right) . \quad (3)$$

Integration over the relative coordinates $\vec{r}_1-\vec{r}_3$, $\vec{r}_2-\vec{r}_4$, and $\vec{r}_1-\vec{r}_2$ then yields a <u>non-symmetrized</u> transition matrix element

$$M(1,2,3,4) = V_G(\pi r_o^2)^{3/2}\exp\left(-r_o^2(\vec{P}_2+\vec{P}_4)^2/4\hbar^2\right)$$

$$\times \Phi_L(\vec{P}_3 - \frac{m_3}{m_1+m_3}\vec{P}_o)\Phi_L(\vec{P}_4) \quad (4)$$

where the momentum wave function $\Phi_L(\vec{P})$ is

$$\Phi_L(\vec{P}) = \int d^3\vec{r}\,\psi_L(r)\exp\left(i\vec{P}\cdot\vec{r}/\hbar\right) \quad (5)$$

The cross section for finding the detected particles in solid angles $\Delta\Omega_1$ and $\Delta\Omega_2$ and lab energy intervals ΔE_1 and ΔE_2 is

$$\frac{d^4\sigma}{d\Omega_1 d\Omega_2 dE_1 dE_2} = \frac{2\pi}{\hbar v_o}\int |M|^2\,\rho\sin\gamma\,d\gamma\,d\phi \quad (6)$$

where v_o is the projectile velocity and ρ, the density of final states,[15,16] is given by

$$\rho = m_1^3 m_3^{3/2} \sqrt{E_1 E_2 \varepsilon} \; / h^9. \qquad (7)$$

ε is the combined energy of the undetected particles in the RCM.

The predictions in our earlier paper were obtained using the non-symmetrized matrix element, Eq. (4), in Eq. (6). Thus, particle 4 was assumed to originate in the target nucleus. Its momentum wave function $\Phi_L(\vec{P}_4)$ is largest when $\vec{P}_4=0$; i.e., when this particle is left at rest in the laboratory. Particle 3 comes from the projectile, and has its greatest Φ_L when it continues with the projectile velocity; this requires appropriate v_c as well as $\gamma=0$. The remaining factors in Eq. (4) describe the amplitude for momentum transfers $\vec{P}_2$ and $\vec{P}_4$ to the target constituents by the interaction potential.

We now recognize the identity of particles 1 and 2, and of 3 and 4. The matrix element of Eq. (4) is therefore replaced by

$$M_{symm} = M(1,2,3,4) + M(1,2,4,3) + M(2,1,3,4) + M(2,1,4,3) \qquad (8)$$

The three additional terms in Eq. (8) are all, strictly speaking, exchange terms. However, we designate the second term as "exchange" and the third and fourth as "potential terms", for the following reason. We find in the next section that any interaction potential of range $r_o \geq 1$ fm significantly displaces the DSP peak from its observed location

but has relatively little effect on its width. We therefore replace the gaussian potential (Eq. 3) by $V_o\delta(\vec{r}_1-\vec{r}_2)$, and Eq. (8) becomes

$$M_{symm} = 2V_o\left(\Phi_L(\vec{P}_3-\frac{m_3}{m_1+m_3}\vec{P}_o)\Phi_L(\vec{P}_4) + \Phi_L(\vec{P}_4-\frac{m_3}{m_1+m_3}\vec{P}_o)\Phi_L(\vec{P}_3)\right) \qquad (9)$$

The distinction between participants, as to which originated in the projectile, has now disappeared, and the effect of including the two potential terms is simply to double the amplitude.

We now show that the exchange term, in which the roles of the spectators are reversed, has only a small effect on the line shape. When Eq. (9) is substituted into Eq. (6), integration limits $0\leq\gamma\leq\pi/2$ are set. $d^4\sigma$ is then doubled to compensate for restricting the angular range, since the exchange term at $\pi-\gamma$ equals the direct term at angle γ, and vice versa. Since $\gamma\leq\pi/2$, $|\vec{P}_3|\geq|\vec{P}_4|$ and consequently $\Phi_L(P_3)\leq\Phi_L(P_4)$. The other factor in the exchange term is smaller than its direct counterpart, for similar reasons. Therefore, the exchange term will influence the energy spectrum, if at all, through interference with the direct term.

Absolute predictions of the cross section are desirable, so we may judge whether the enhancements observed in our spectra are the result of QFS under double spectator conditions or some other, more improbable, effect. However, it is not clear which constants V_g and r_o (or V_o) should determine the interaction potential, since no potential as simple

as Eq. (3) has been used to analyze either α-α or d-d elastic scattering. One approach is to calculate the elastic scattering cross section, $(d\sigma/d\Omega)$, by the same procedures as the double breakup cross section $d^4\sigma$, and then use the measured $(d\sigma/d\Omega)$ to predict $d^4\sigma$. Kuckes et al.[1] proceeded similarly and found that the ratio of the nucleon-deuteron QFS breakup cross section to the nucleon-nucleon elastic cross section was given more accurately by the PWBA theory than was either individual cross section. We perform such a calculation, assuming that the participants interact through a δ-function potential, and find

$$\frac{d^4\sigma}{d\Omega_1 d\Omega_2 dE_1 dE_2} = \frac{1}{\hbar^6}\left(\frac{d\sigma}{d\Omega}\right)_{c.m.} P_{\alpha d}^2\, m_1 m_3 (m_0 m_3 E_1 E_2 \epsilon / E_0)^{1/2}$$

$$\times \int \left[\Phi_L(\vec{P}_3 - \frac{m_3}{m_1+m_3}\vec{P}_0)\Phi_L(\vec{P}_4) + \text{exchange}\right]^2 d\Omega_\epsilon \ . \qquad (10)$$

In Eq. (10), m_o and E_o are the mass and lab energy of the projectile, and $P_{\alpha d} = 0.54$ is the probability that each initial ^{6}Li nucleus will have α+d cluster structure.[9]

Eq. (10) is used to predict $d^4\sigma$ for four sets each of α-α and d-d QFS scattering data reported in I, and the results are given in Table 1. The angle pair chosen, for each projectile energy E_o, is the one whose kinematics most closely resemble those for elastic scattering of the participants at 90° in their own c.m. frame. Thus, comparisons are made by interpolating α-α elastic scattering data[17,18] at 90° c.m. to lab energy 2/3 E_o. d-d elastic scattering data were needed from 12.1 to 15.5 MeV (i.e., at $E_o/3$) but published data exist only at the bottom of this range. However, the

90.13° excitation function[19] varies smoothly from 3.5 to 12.25 MeV, and is well fitted by the empirical formula

$$\left(\frac{d\sigma}{d\Omega}\right)_{d-d} = (167 - 6.2\ E\ (\text{MeV}))\ \text{mb/sr} \qquad (11)$$

from 9 to 12.25 MeV. Therefore $(d\sigma/d\Omega)_{d-d}$ was calculated from Eq. (11), which presumably gives an acceptable estimate of $d^4\sigma$.

The "total measured $d^4\sigma$" values in Table 1 represent the maximum yield at each E_o and θ. The spectra displayed in I show DSP enhancements rising above a roughly energy-independent background, presumably caused by other reaction mechanisms. An estimate of this background has been subtracted to give the "net measured $d^4\sigma$" values.

The maximum predicted $d^4\sigma$'s for α-α QFS are comparable to the measured values, although there are tendencies for the measured values to rise and the predicted ones to fall with increasing energy. Since, as we show later, the predicted peaks are typically 5 times wider than the measured ones, the predicted total yield is greater than, but of the same order of magnitude as, the observed yield. For d-d QFS the two total yields are quite comparable, since the measured maxima are 2.4 to 4 times the predicted ones.

The PWBA therefore correctly predicts both the positions of the DSP enhancements (unless a participant interaction potential of too long range is assumed) and the order of magnitude of their strength. However, in the next four sections, we find no way to modify the theory so as to explain their remarkably small widths.

3. Exchange Effects

The matrix elements used in I were not symmetrized in the coordinates of the two deuterons and the two α-particles. Therefore, we should see whether symmetrization affects the predicted peak widths, which are far too large in the non-symmetrized theory. DSP line-shape calculations for both d-d and α-α QFS are presented in Fig. 2.; curves labelled σ_o omit the exchange term in Eq. (9), and those labelled $\Delta\sigma_{ex}$ show its (entirely negligible) contribution to the cross section. These calculations assumed a δ-function participant interaction potential, and the α-d momentum wave function was obtained for a Woods-Saxon potential

$$V_{\alpha d}(r) = V_o \left[1 + \exp\left(\frac{r-R_o}{a}\right)\right]^{-1} \qquad (12)$$

with R_o = 5 fm and a = 3 fm. This notably long range potential gives an rms cluster separation of 6.15 fm, much greater than the accepted ^{6}Li charge radius[20] of about 2.5 fm. Nevertheless, it predicts peaks much wider than those observed, and decreasing R_o would further increase their width. A well depth V_o = -5.1360 MeV, just slightly greater than that needed for the binding energy of 1.473 MeV, was used. Since the numerically-integrated $\psi_L(r)$ eventually diverges at large r, the integration in Eq. (5) was terminated at the radius where $\psi_L(r)$ changed sign. All results of our calculations were verified to be stable against changing V_o by its computational uncertainty.

The exchange term in Eq. (9) is largest when $\vec{P}_3$, and $\vec{P}_4$ minus m_3 times the projectile velocity, are smallest.

From Fig. 1, this happens when $\gamma = \pi/2$; i.e., at the upper limit of integration in Eq. (6). At the DSP peaks of Fig. 2, these momenta are about 150 MeV/c and 300 MeV/c for α-α and d-d QFS, respectively. Figure 3 shows that $\Phi(P)$ is very small for such large momenta, so it follows that exchange effects are negligible. Moreover, the exchange contributions come from a region where $\Phi(P)$ for the Woods-Saxon potential alternates in sign, further reducing their effect.

These results contrast with those of Phillips,[21] who showed that symmetrization narrows sequential decay peaks from the ^{8}Be first excited level observed in the ^{11}B(p,3α) reaction, in comparison with those observed in α-α elastic scattering. His experiments differ from ours in at least two important aspects: the bombarding energy (E_p ~ 3 MeV) is lower, and the reaction mechanism (sequential decay vs. a presumed direct double breakup reaction) is different.

In our model, exchange effects on both the line shape and the absolute cross section are negligible and they decrease with increasing bombarding energy. It would be difficult to perform an experiment at a sufficiently low energy (E_o ~ 5 to 10 MeV) to observe these effects.

4. Coulomb Effects

The peaks observed in I involve typical spectator momenta ≤20 MeV/c. The Coulomb barrier extends to 30 fm when a deuteron with this momentum interacts with an α-particle. The Coulomb potential influences the wave function throughout this wide barrier region and will therefore affect the line shape.

Wave functions were obtained for clusters interacting through a Woods-Saxon nuclear potential and the Coulomb potential of a uniformly charged sphere of radius 3 fm. The binding energy and rms cluster separation maintained their previously-quoted values with nuclear potential parameters V_o = -6.496 MeV, R_o = 5 fm, and a = 3 fm.

Figure 2 shows that adding the Coulomb potential slightly increases the predicted width. Curves for both potentials have the same arbitrary normalization factor; thus, the Coulomb force primarily reduces the yield for very small spectator momenta. Figure 3 shows that momentum wave functions for the two potentials differ significantly only at small p. This difference results from the increased "roughness" of the Coulomb spatial wave function, due to the deeper nuclear well and the long-range Coulomb force.

5. Effects of Participant Interaction Potential

The effect on the line shape of varying the force range r_o (Eq. 3) is shown in Fig. 4. This quantity was varied because it is one of the few adjustable parameters in the extended PWBA theory, and because the effects of this potential may crudely simulate those of distorted waves for the participants, which would be much harder to incorporate. Cluster wave functions were obtained for a pure nuclear potential (V_o = -2.56 MeV, R_o = 12 fm, a = 3 fm) of longer range than was used previously. This was done to obtain peaks slightly less wide than those in Fig. 2, for easier estimation of their centroids; nevertheless the predicted peaks are still far too wide. The peak width was found to be nearly independent of r_o, but its center deviates appreciably from the observed center when $r_o \geq 1$ fm. A δ-function interaction potential was therefore used in all of our other calculations.

6. Deuteron Structure Effects

Until now, the α+d clusters in ^{6}Li have been treated as geometric points. There are good reasons why their structure, especially that of the deuteron, may influence the reaction mechanism and therefore the momentum distribution of the clusters emerging from double breakup. For example, if two deuterons are to remain after α-α QFS they should have looked like deuterons in the initial ^{6}Li nuclei; i.e., they should have been far enough from the α-particles not to have been distorted by their nuclear force fields. Since

the deuteron is such a large object, it should also be far from the α-particle to avoid re-scattering after the primary QFS event. Finally, one may expect nucleon exchange between deuterons, though this should be less likely for the tightly-bound nucleons in the α-particle.

Deuteron structure is included in the extended PWBA model by treating each deuteron as two nucleons with a relative wave function

$$D(i,j) = \sum_{s=1}^{3} A_s \exp\left(-\eta_s^2(\vec{r}_i-\vec{r}_j)^2\right)S_1^m T_o^o \qquad (13)$$

The three-component Gaussian function in Eq. (13) has been given by van Oers and Slaus;[22] it is used in preference to the Hulthen and other functions to simplify the calculations which follow. S_1^m and T_o^o are the spin and charge wave functions for the two nucleons. Calculations have proven feasible only for α-α QFS, and only when the participant α's interact through a δ-function potential. We therefore start with a matrix element

$$M_o = \langle F|V_o\delta(\vec{r}_a-\vec{r}_b)|I\rangle \qquad (14)$$

where

$$\langle F| = D(i,j)D(k,l)\exp\{i(\vec{P}_{ij}\cdot\vec{R}_{ij} + \vec{P}_{kl}\cdot\vec{R}_{kl} + \vec{P}_a\cdot\vec{R}_a + \vec{P}_b\cdot\vec{R}_b)\} \qquad (15)$$

and

$$|I\rangle = L(ij,a)L(kl,b)D(i,j)D(k,l)\exp\{i(\vec{P}_o\cdot\vec{R}_{ij,a})\} \qquad (16)$$

Indices i,j,k and l designate the nucleons in the deuterons, and a and b represent the α-particles. The ^{6}Li cluster

wave functions L (ij,a), etc., are single-component Gaussian functions to make our calculations tractable.

The basic matrix element described in Eqs. (14) through (16) is represented in compact notation as

$$M_o = \langle ij,a;kl,b|ij,a;kl,b\rangle \qquad (17)$$

The effects of nucleon exchange must now be considered. It is sufficient[23,24] to antisymmetrize either the initial or the final state, and we choose the former. Since the deuteron wave functions already have internal asymmetry, we need to exchange nucleons only between deuterons. We thus obtain 4!/(2! x 2!) = 6 matrix elements, including

$$M_2 = \langle ij,a;kl,b|kl,a;\ ij,b\rangle\ , \qquad (18)$$

and four of type

$$M_1 = \langle ij,a;\ kl,b|jk,a;\ li,b\rangle\ . \qquad (19)$$

The subscript on each M tells how many nucleon exchanges are involved. Writing the indices as a cyclic permutation of (ijkl) insures that all M's appear with proper phase[24,25] in expressions involving their sum.

The zero and two-nucleon exchange elements M_o and M_2 represent exactly the same physical processes as the two terms of Eq. (9) and are even simpler to evaluate since the wave functions, previously obtained numerically for the Woods-Saxon potential, can now be found analytically for the gaussian wave function L(ij,a). The single-exchange

element M_1 is far more complicated, involving coupled integrations over three radial coordinates. We do not need its specific functional form, and omit the formula for it to save space. We average over initial states of the system and sum over final states, obtaining

$$\frac{d^4\sigma}{d\Omega_1 d\Omega_2 dE_1 dE_2} = \frac{2\pi\rho}{9\hbar v_o} \int (5(M_o - 2M_1 + M_2)^2 + 3(M_o + M_2)^2 + 1(M_o + M_1 + M_2)^2) \sin\gamma d\gamma d\phi \qquad (20)$$

At each angle γ, the cross section involves coherent sums of the spatial matrix elements,[24] but the various spin states add incoherently since projectile, target, and reaction products are unpolarized.

DSP line-shape calculations from Eq. (20) are indistinguishable from those of the Woods-Saxon potential, with Coulomb forces and deuteron structure neglected (Fig. 2, curves labelled σ_o). The reason is illustrated in Fig. 5 where the three spatial matrix elements are plotted vs. the d-d emission angle γ. This figure shows the very strong forward peaking of the direct term M_o, due to the rapid increase with γ of the spectator momentum; it also shows that M_o and the deuteron-exchange term M_2 play complementary roles in the two hemispheres. M_1, a non-spectator term, is nearly isotropic in the RCM; it selects a very wide range of momentum components, since the region of overlap of the four deuteron and two ^{6}Li wave functions of the initial and final states is quite small. We note that it is the

dominant term at 90°; any model which assigns greater importance to single nucleon exchange will therefore predict even broader peaks.

The ^{6}Li gaussian cluster wave function used for Fig. 5 gives an rms cluster separation of 6.2 fm, equal to that of the Woods-Saxon potential used earlier. Figure 6 shows the dependence of DSP peak width upon $\langle r^2 \rangle^{1/2}$. We see that separations of about 30 fm are required to produce the unexpectedly small (~1 MeV) widths of the observed peaks. This is consistent with the artificially long cutoff of the wave functions used in I for fitting purposes.

The immemse cluster separation required to reproduce the widths is reminiscent of nucleon-deuteron breakup calculations by Paić et al.[26] They fitted the QFS peaks by excluding contributions from nucleons separated by less than 3 to 6 fm in the deuteron. However, such a cutoff radius is comparable to the deuteron radius, and is reasonable since inside this radius more complicated processes than QFS may dominate.

7. Summary and Conclusions

The PWBA correctly predicts both the location and the approximate strengths of the peaks attributed in I to double spectator pole processes. However, the predicted widths remain about five times too large even after all obvious straight-forward improvements -- symmetry under Boson exchange, Coulomb cluster wave functions, a finite-range participant

interaction potential, and deuteron structure -- are added to the model. This work, moreover, anticipates some problems which more sophisticated models may not overcome. For example, diagrams involving nucleon exchange are not spectator processes; their overlap integrals are confined to the α-particle and/or deuteron volumes, and they broaden the momentum distribution. Nor do distorted waves, allowing for the attractive participant interaction potential, offer any obvious way to limit the collisions to highly peripheral ones consistent with atypically small spectator momenta.

Realistic ^{6}Li wave functions predict that only a small fraction of clusters are separated far enough to give the observed momentum distribution; thus the large strength of the reaction, 100% of the PWBA prediction, is quite puzzling.

More experimental data are needed to determine the reaction mechanism. The rarity of intermediate-momentum DSP events may result from rescattering of participants by spectators. This effect should be most severe at QFS c.m. scattering angles near 90°, where the data of I were taken, and so angular distributions extending to small angles are desirable. Angular distributions for both spectators and participants, requiring a large detector array, would be useful since double coincidence measurements do not determine the spectator emission angles γ,ϕ. The peaks reported in I were shown not to result from final-state interactions, which yield participant-spectator pairs with close angular correlation. They are consistent with either DSP events

(undetected clusters strongly forward-peaked in the RCM) or isotropy in the RCM. The latter distribution might identify a (clearly speculative and improbable) process such as the initial excitation of both ^{6}Li nuclei to virtual levels near the α-d continuum, favoring low-momentum components, followed by QFS of the participants.

To establish a relationship between these phenomena and participant-spectator processes in heavier nuclei, the widths should be measured for higher bombarding energies, and the final state ^{3}He + ^{3}He + 2t should be studied well above its 63 MeV threshold energy. Observation of collisions between ^{6}Li and another light nucleus, or between two light nuclei with A > 6, would indicate whether this phenomenon is general or specific to the ^{6}Li nucleus.

I wish to thank Professors G. Bertsch and D.K. Scott for their general interest and careful reading of this manuscript, Professor B.H. Wildenthal for helpful suggestions regarding the computations, and J. Ortiz for programming assistance.

References

1. A.F. Kuckes, R. Wilson, and P.F. Cooper, Jr., Annals of Phys. 15 (1961) 193.
2. P.G. Roos, D.A. Goldberg, N.S. Chant, R. Woody, and W. Reichart; Nucl. Phys. A257 (1976) 317.
3. I. Slaus, R.G. Allas, L.A. Beach, R.O. Bondelid, E.L. Petersen, J.M. Lambert, and D.L. Shannon; Phys. Rev. C3 (1973) 444.
4. R.E. Warner, G.C. Ball, W.G. Davies, A.J. Ferguson, and J.S. Forster; Phys. Rev. Letters 27 (1971) 961.
5. C.-K. Gelbke, M. Buenerd, D.L. Hendrie, J. Mahoney, M.C. Mermaz, and D.K. Scott, Phys. Reports 42 (1978) 312.
6. Ch. Engelhaaf, G. Bohlen, H. Fuchs, A. Gamp, H. Homeyer, and H. Kluge, Phys. Rev. Lett. 46 (1981) 813.
7. D.K. Scott, Lectures presented at the International School on Nuclear Physics, Alushta, Crimea, USSR, 1980 (unpublished); Michigan State University Report MSUCL-326.
8. A.S. Goldhaber, Phys. Lett. 53B (1974) 306.
9. J.V. Noble, Phys. Lett. 55B (1975) 433.
10. B. Neumann, H. Rebel, J. Buschmann, H.J. Gils, H. Klewe-Nebenius and S. Zagromski, Z. Phys. A296 (1980) 113.
11. R.E. Warner, G.C. Ball, W.G. Davies, and J.S. Forster, Nuclear Physics A (to be published).
12. K.W. McVoy and M.C. Nemes, Zeits. Phys. A295 (1980) 177.

13. R.E. Warner, D.C. Martin, G.C. Ball, W.G. Davies, A.J. Ferguson, and D. Horn; Nucl. Phys. A326 (1979) 209.
14. D.C. Martin, Senior honors thesis, Oberlin College (1978) unpublished.
15. M. Furic and H.H. Forster, Nucl. Instr. 98 (1972) 301.
16. W.S.C. Williams, An Introduction to Elementary Particles, 2nd edition (Academic Press, 1971) pp. 499-504.
17. W.S. Chien and R.E. Brown, Phys. Rev. C10 (1974) 1767.
18. A.D. Bacher, F.G. Resmini, H.E. Conzett, R. de Swiniarski, H. Meiner, and J. Ernst; Phys. Rev. Lett. 29 (1972) 1331.
19. A.S. Wilson, M.C. Taylor, J.C. Legg, and G.C. Phillips, Nucl. Phys. A126 (1969) 193.
20. D.A. Sparrow and W.J. Gerace, Nucl. Phys. A145 (1970) 289.
21. G.C. Phillips, Rev. Mod. Phys. 37 (1965) 409.
22. W.T.H. van Oers and I. Slaus, Phys. Rev. 160 (1967) 853.
23. W. Tobocman, Direct Nuclear Reactions (Oxford University Press, 1961).
24. R.E. Warner and E.W. Vogt, Nucl. Phys. A204 (1973) 433.
25. D.U.L. Yu and W.E. Meyerhof, Nucl. Phys. A80 (1966) 481.
26. G. Paić, J.C. Young, and D.J. Margaziotis, Phys. Letters B32 (1970) 437.

Figure Captions

FIG. 1. Geometry for double coincidence detection of $^6Li + {}^6Li \rightarrow 2\alpha + 2d$ reaction.

FIG. 2. a. Predicted and measured α-α coincidence cross sections for $^6Li + {}^6Li \rightarrow 2\alpha + 2d$ reaction. Data are from (ref.[11]), and $|E_{\alpha 1} - E_{\alpha 2}| \leq 1$ MeV. σ_o denotes prediction for pure nuclear α-d interaction, and σ_{coul} includes both nuclear and Coulomb forces.

b. Similar to a., for d-d coincidence cross sections.

FIG. 3. ^6Li cluster momentum wave functions for pure nuclear (Φ_o) and nuclear plus Coulomb (Φ_{coul}) interactions.

FIG. 4. DSP line-shape predictions for different ranges of participant interaction potential.

FIG. 5. Matrix elements for zero-, one-, and two-nucleon exchange between deuterons, vs. spectator deuteron RCM emission angle γ, for α-α QFS.

FIG. 6. Width of double spectator peak vs. rms separation of α+d clusters (gaussian cluster wave function).

Table 1. Measured and predicted $^6Li + {}^6Li$ double breakup cross sections

E_o MeV	(deg)	Type	Measured $d^4\sigma$ mb/(sr^{2}Mev^2) Total	Net	$(d\sigma/d\Omega)_{c.m.}$ (mb/sr)	Predicted $d^4\sigma$ mb/(sr^{2}Mev^2)
36.4	41.0	α-α	10.4	6.4	49	1.6
39.4	41.4	α-α	8.3	5.4	136	4.4
43.0	41.7	α-α	7.7	4.8	206	6.7
46.6	42.0	α-α	5.0	2.7	210	7.0
36.4	41.0	d-d	2.9	2.0	91	0.55
39.4	41.4	d-d	2.8	2.1	85	0.52
43.0	41.7	d-d	1.8	1.2	78	0.51
46.6	42.0	d-d	2.0	1.6	70	0.45

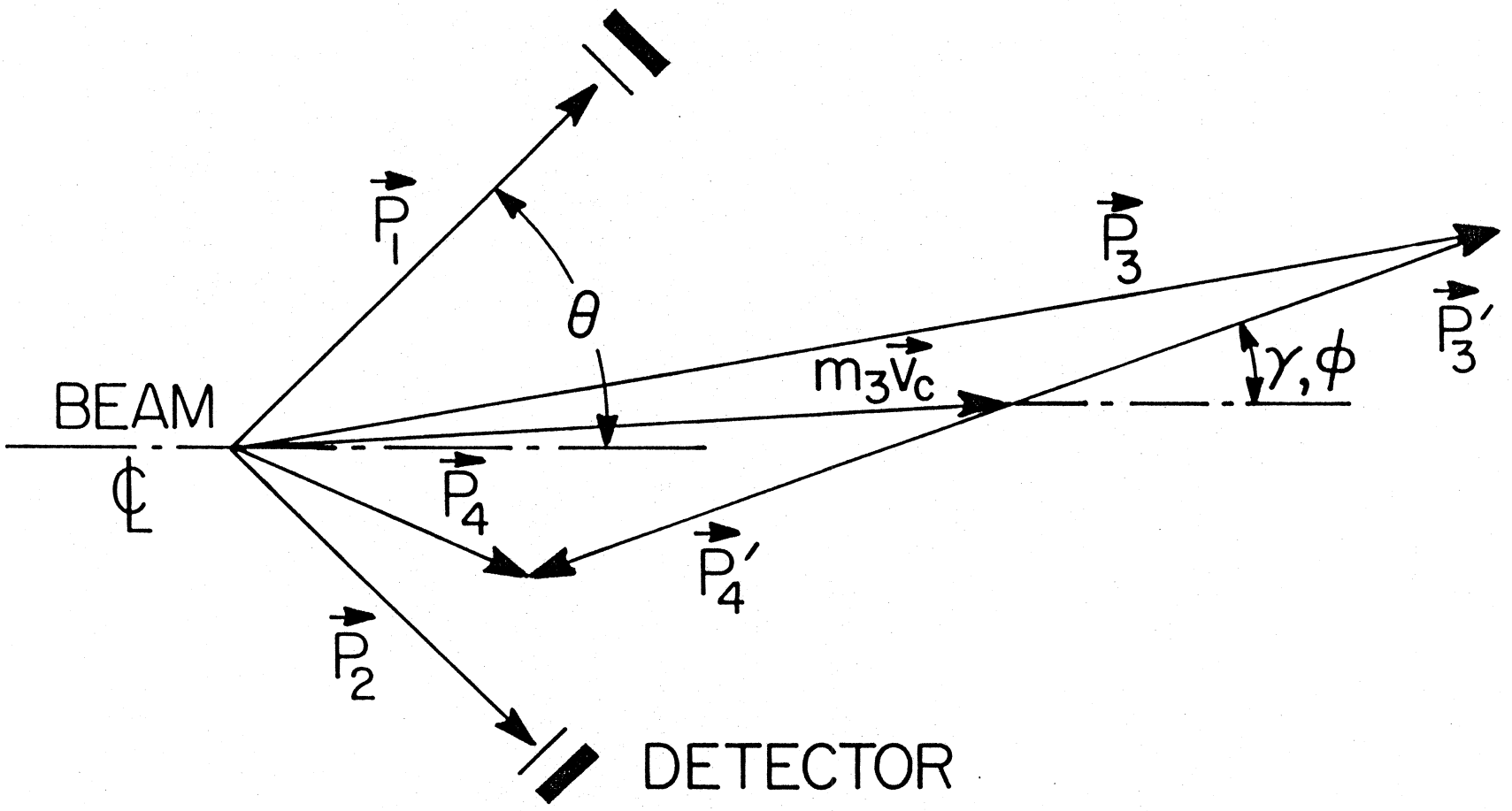
$\vec{P}_1$
θ
$\vec{P}_3$
$\vec{P}_3'$
$m_3\vec{v}_c$
γ, ϕ
BEAM
$\vec{P}_4$
$\vec{P}_4'$
$\vec{P}_2$
DETECTOR

FIG. 1

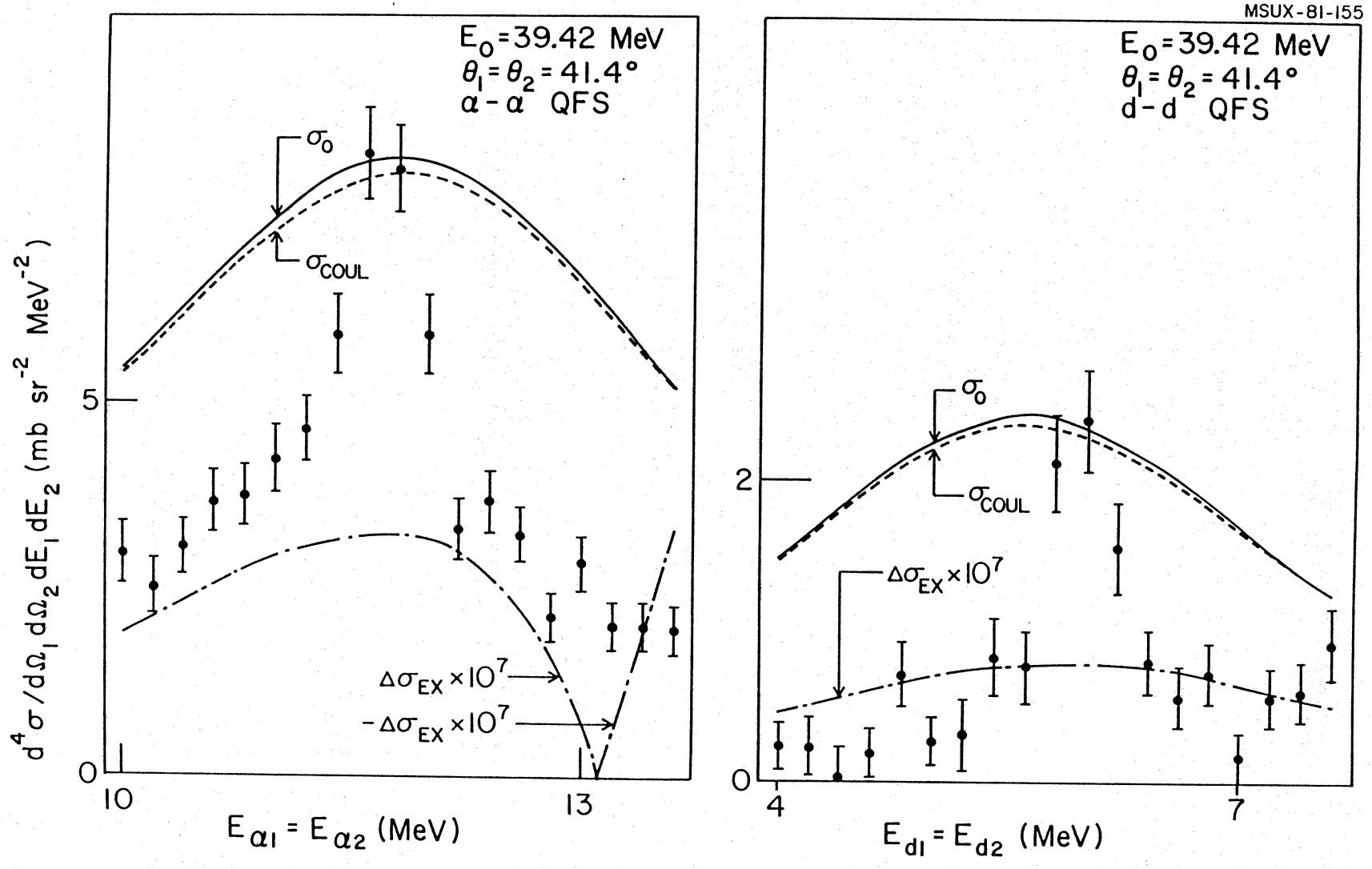
E0=39.42 MeV
θ1=θ2=41.4°
α-α QFS
σ0
σCOUL
ΔσEX×10^7
-ΔσEX×10^7
d^4σ/dΩ1dΩ2dE1dE2 (mb sr^-2 MeV^-2)
5
0
10
13
Eα1 = Eα2 (MeV)
E0=39.42 MeV
θ1=θ2=41.4°
d-d QFS
σ0
σCOUL
ΔσEX×10^7
2
0
4
7
Ed1 = Ed2 (MeV)

FIG. 2

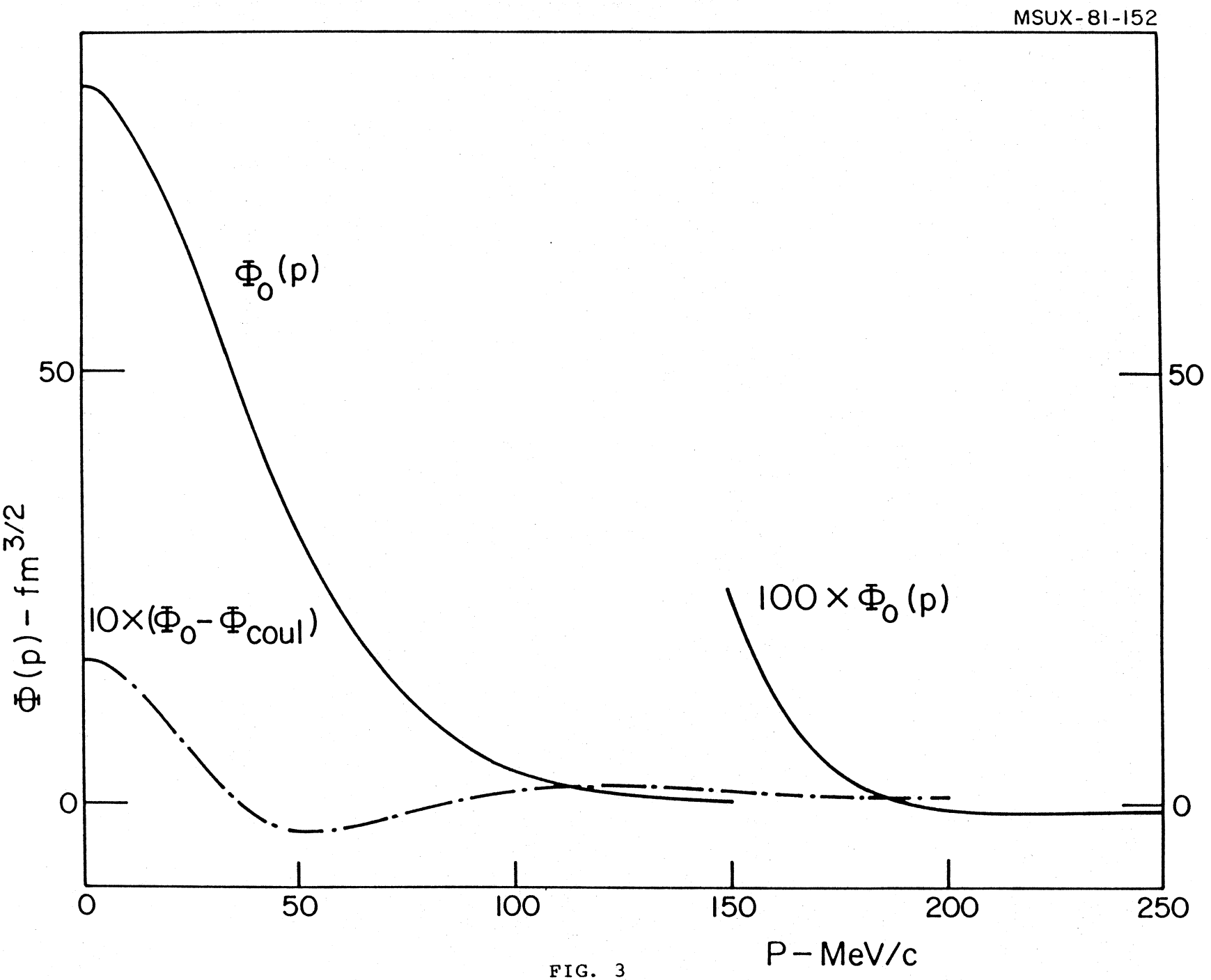
MSUX-81-152
$\Phi_0(p)$
$10\times(\Phi_0-\Phi_{coul})$
$100\times\Phi_0(p)$
$\Phi(p)$ - fm$^{3/2}$
50
0
50
0
0
50
100
150
200
250
P - MeV/c

FIG. 3

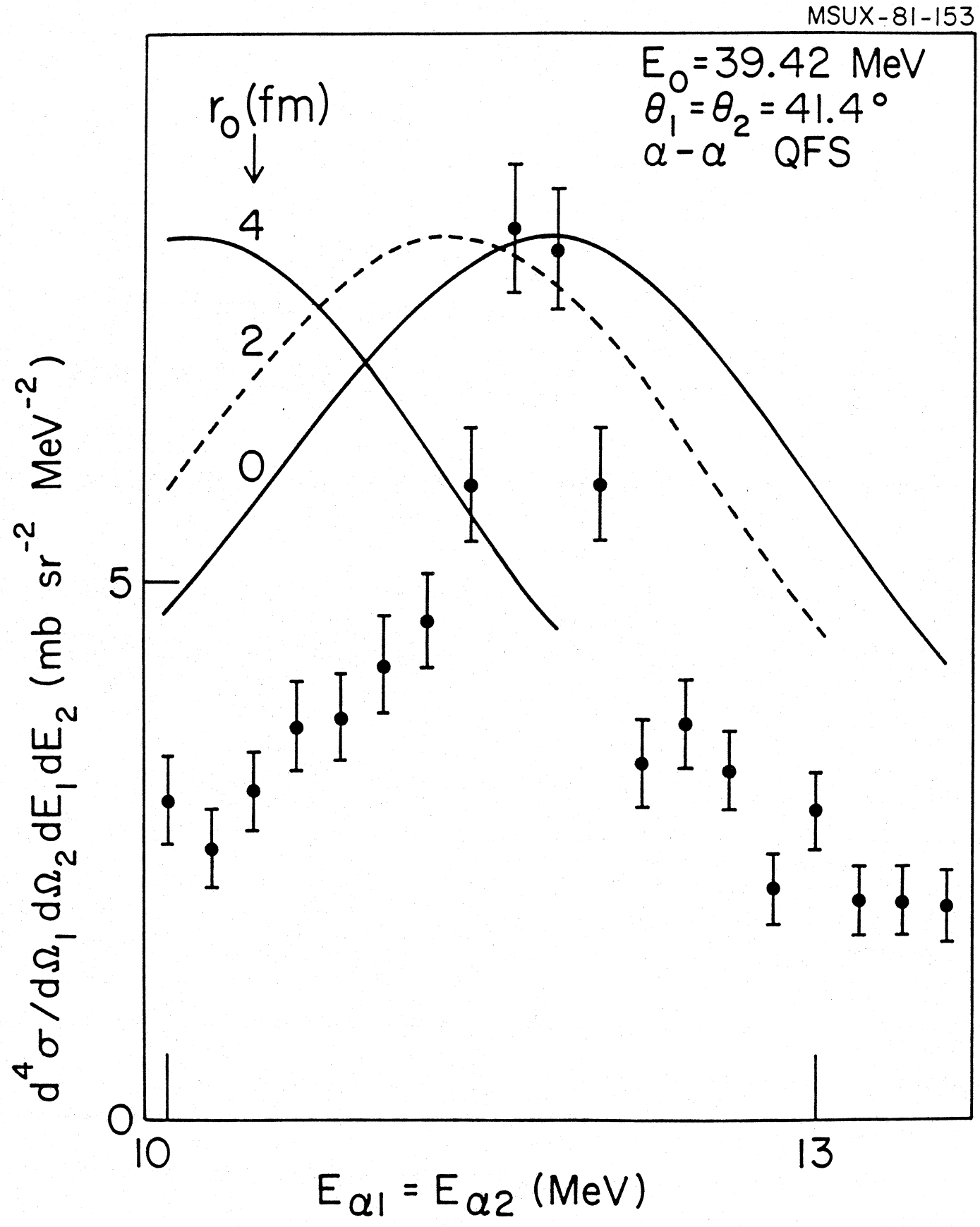
MSUX-81-153
$E_0 = 39.42$ MeV
$\theta_1 = \theta_2 = 41.4°$
$\alpha - \alpha$ QFS
r_0(fm)
4
2
0
5
0
10
13
$d^4\sigma/d\Omega_1 d\Omega_2 dE_1 dE_2$ (mb sr^{-2} MeV^{-2})
$E_{\alpha 1} = E_{\alpha 2}$ (MeV)

FIG. 4

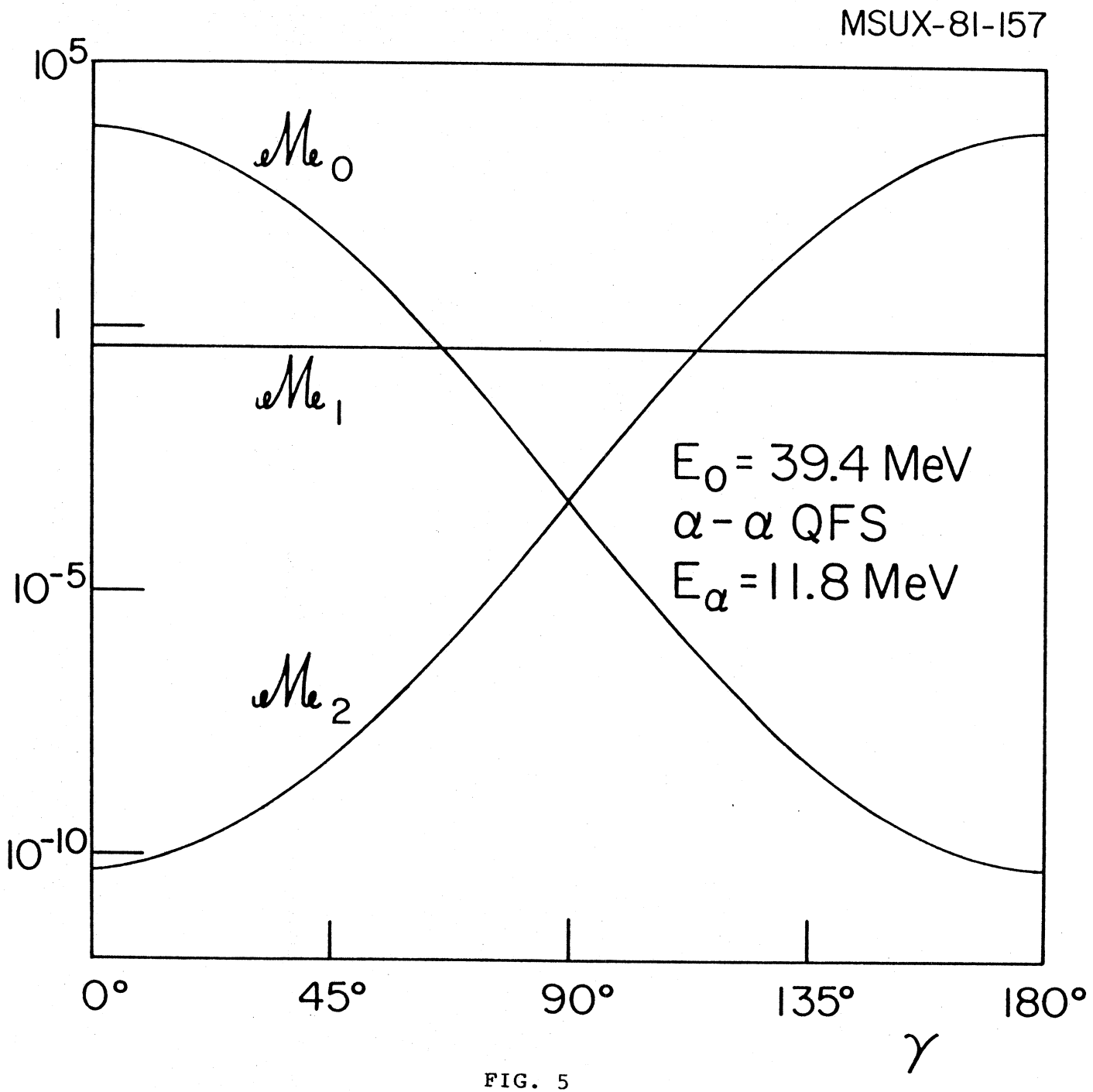
MSUX-81-157
10^5
1
10^{-5}
10^{-10}
$\mathcal{M}e_0$
$\mathcal{M}e_1$
$\mathcal{M}e_2$
$E_0 = 39.4$ MeV
$\alpha - \alpha$ QFS
$E_\alpha = 11.8$ MeV
0°
45°
90°
135°
180°
γ

FIG. 5

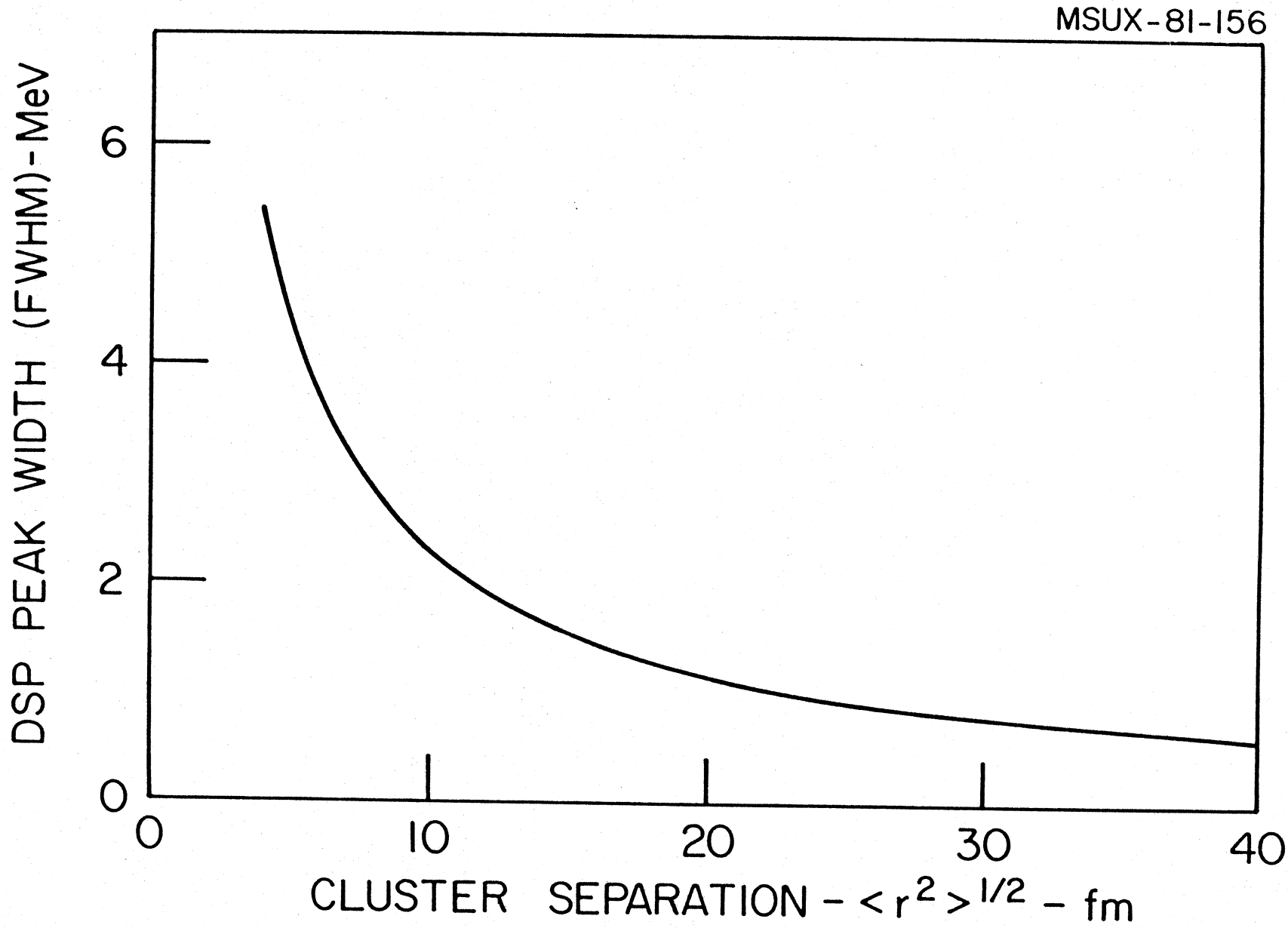
MSUX-81-156
DSP PEAK WIDTH (FWHM)-MeV
0
2
4
6
0
10
20
30
40
CLUSTER SEPARATION - $\langle r^2 \rangle^{1/2}$ - fm

FIG. 6